Associated Sectors of Magnetic Recording Systems Using Spatially Coupled LDPC Codes

Sirawit Khittiwitchayakul, Non-member,
Watid Phakphisut†, and **Pornchai Supnithi**, Members

ABSTRACT

In traditional magnetic recording systems, non-associated sectors are mainly adopted, whereby two consecutive sectors are decoded independently by the low-density parity-check (LDPC) codes. In this paper, we propose a magnetic recording system with associated sectors, constructed using spatially coupled low-density parity-check (SC-LDPC) codes. If the SC-LDPC decoder cannot correct the erroneous bits in the current sector, it can request information stored in previous sectors to improve decoding performance. Moreover, we modify protograph-based extrinsic information transfer (P-EXIT) charts to examine the theoretical performance of SC-LDPC codes applied to both non-associated and associated sectors. Our theoretical results show that the associated sectors achieve significant performance gains compared to the traditional non-associated sectors.

Keywords: Spatially Coupled Low-Density Parity-Check Codes, SC-LDPC, Non-Associated Sectors, Associated Sectors, Bit Pattern-Media Magnetic Recording System, BPMR, Protograph-Based Extrinsic Information Transfer Chart, P-EXIT

1. INTRODUCTION

Spatially coupled low-density parity-check (SC-LDPC) codes [1] are proven to achieve the maximum posteriori (MAP) decoding thresholds of their underlying LDPC codes [2–3]. However, they require long codewords, resulting in high decoding complexity. The window decoding method is suitable for SC-LDPC codes [4], whose decoding complexity and latency can be restricted. Moreover, Iyengar *et al.* show that the window decoding threshold approaches the belief propagation threshold as the window size grows [5]. As a result, SC-LDPC codes for future high-density magnetic recording systems have received considerable interest [6–8], providing both high efficiency and low complexity. In [6], Esfahanizadeh *et al.* proposed a design structure for SC-LDPC codes to correspond to the characteristics of magnetic recording channels. Similarly, in [7], Yang *et al.* proposed SC-LDPC code design for two-dimensional magnetic recording (TDMR) systems using a turbo detection configuration. Both approaches [6–7] offer significant performance gains over conventional SC-LDPC codes. In our prior work [8], the reduced-complexity window decoding of SC-LDPC codes has been introduced into bit pattern-media magnetic recording (BPMR) systems.

In traditional magnetic recording systems, the user bits are divided into multiple blocks, with each block being encoded and recorded in its own data sector. This recording mechanism can be viewed as non-associated. Hence, in [6–8], when the SC-LDPC codes cannot correct the erroneous bits in the current sector, the decoded information from the previous sectors cannot be used to aid it. Recently, Esfahanizadeh *et al.* introduced a collaboration among neighboring sectors with different signal-to-noise ratios (SNRs) in additive white Gaussian noise (AWGN) channels [9]. The results reveal that well-designed SC-LDPC codes are more robust against SNR variations than traditional LDPC codes.

In this paper, the use of SC-LDPC codes is proposed to construct associated sectors, where recorded data from previous sectors can be requested to combat erroneous bits in the current sector. In contrast to the method in [9], in this study we consider the mechanisms of magnetic recording systems, whereby the previous sectors are reread when the SC-LDPC decoder cannot correct the erroneous bits in the current sector. This approach can be carried out using window decoding. Moreover, we modify the P-EXIT charts [10] to analyze the theoretical performance (i.e., decoding threshold) of the SC-LDPC codes with window decoding in both non-associated and associated sectors. The theoretical results show that the decoding thresholds of non-associated sectors are superior to those in the associated sectors (without aiding). However, when the recorded data in the previous sector are requested, the decoding thresholds of the associated sectors have the opposite tendency, evidently outperforming the non-associated sector. These theoretical analyses in bit pattern-media magnetic recording (BPMR) systems confirm our preliminary studies in [11].

The remainder of the paper is organized as follows. In Section 2, the SC-LDPC codes and their window decoding are briefly discussed. The SC-LDPC code used in magnetic recording systems is explained in Section 3. In Section 4, we discuss the non-associated

Manuscript received on May 15, 2021; revised on August 24, 2021; accepted on August 26, 2021. This paper was recommended by Associate Editor Piya Kovintavewat.

The authors are with the School of Engineering, King Mongkut's Institute of Technology Ladkrabang, Bangkok 10520, Thailand.

†Corresponding author: watid.ph@kmitl.ac.th

Digital Object Identifier: 10.37936/ecti-eec.2022201.246094

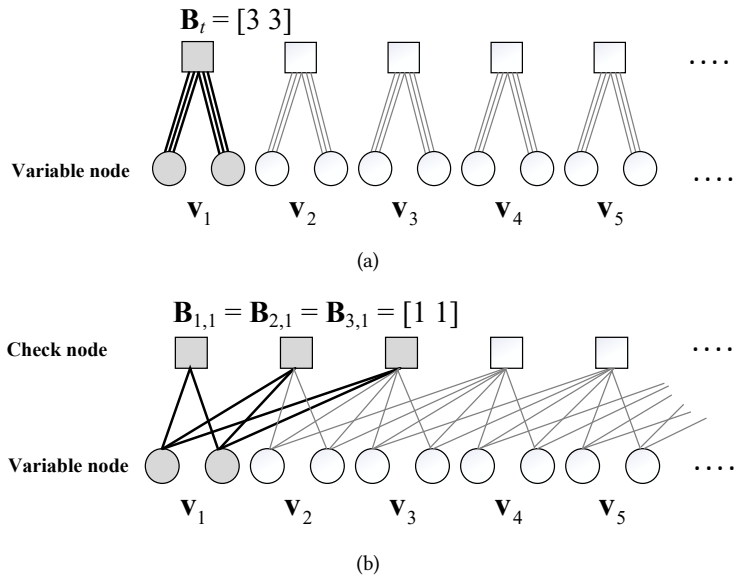

Fig. 1: *Protographs of (a) the traditional LDPC code with the base matrix $\boldsymbol{B}_t = [3\ \ 3]$ and (b) SC-LDPC code with the base matrix $\boldsymbol{B}_{1,t} = \boldsymbol{B}_{2,t} = \boldsymbol{B}_{3,t} = [1\ \ 1]$.*

and associated sectors of magnetic recording, as well as their theoretical analysis. The results of the theoretical analysis are presented in Section 5. The computer-based simulations are then presented to confirm the theoretical results in Section 6, while Section 7 concludes the study.

2. SPATIALLY COUPLED LOW-DENSITY PARITY-CHECK (SC-LDPC) CODES

2.1 Definition and Notation

Protographs [12], blueprints for constructing LDPC codes, are widely used to evaluate the theoretical decoding threshold under the belief propagation decoding of LDPC codes. The protograph of LDPC codes at time, t, can be written as a base matrix, $\mathbf{B}_t$, size is $n_c \times n_v$, where n_c is the number of check nodes, and n_v is the number of variable nodes in the protograph. Thus, the codeword for the protograph at time, t, consists of the variable nodes, $\mathbf{v}_t = \left[v_1, v_2, \ldots, v_{n_v}\right]$. The parity-check matrix, $\mathbf{H}_t$, of LDPC codes, can be obtained by replacing the non-zero elements of $\mathbf{B}$ with $M \times M$ permutation matrices, and zero elements with $M \times M$ zero matrices. To construct the protograph of SC-LDPC codes, the LDPC codewords at different times must be connected in a chain [13], where the edges of the variable nodes of the protograph at time, t, are connected to the check nodes of the protograph at times, $t + s - 1$, $s = 1, 2, \ldots, m_{cc} + 1$. The memory, m_{cc}, defines the maximum distance between two connected codewords. To maintain the degree of distribution in an original protograph, a derived matrix must satisfy the condition $\sum_{s=1}^{m_{cc}+1} \mathbf{B}_{s,t} = \mathbf{B}_t$. Hence, the base matrix, $\mathbf{B}$ of SC-LDPC codes, measuring $n_c L \times n_v L$, can be written as

$$\mathbf{B} = \begin{bmatrix} \mathbf{B}_1 & \cdots & \mathbf{B}_t & \cdots & \mathbf{B}_{L-2} & \mathbf{B}_{L-1} & \mathbf{B}_L \end{bmatrix}$$
$$= \begin{bmatrix} \mathbf{B}_{1,1} & & & & & & \\ \mathbf{B}_{2,1} & \ddots & & & & & \\ \vdots & \vdots & \mathbf{B}_{1,t} & & & & \\ \mathbf{B}_{m_{cc}+1,1} & \vdots & \mathbf{B}_{2,t} & \ddots & & & \\ & \ddots & \vdots & \vdots & \mathbf{B}_{1,L-2} & & \\ & & \mathbf{B}_{m_{cc}+1,t} & \vdots & \mathbf{B}_{2,L-2} & \mathbf{B}_{1,L-1} & \\ & & & \ddots & \mathbf{B}_{3,L-2} & \mathbf{B}_{2,L-1} & \mathbf{B}_{1,L} \end{bmatrix} \quad (1)$$

where L is the coupling length. The code rate of SC-LDPC codes is

$$R_{SC} = 1 - \frac{n_c}{n_v}. \quad (2)$$

Fig. 1 shows an example of SC-LDPC code, which is built from the traditional LDPC code with $\mathbf{B} = [3\ \ 3]$. Hence, the base matrix, $\mathbf{B}$, can have $\mathbf{B}_{1,t} = \mathbf{B}_{2,t} = \mathbf{B}_{3,t} = [1\ \ 1]$.

2.2 Window Decoding and Rate-Loss Issue

The base matrix in Eq. (1) has a diagonal band of non-zero entries, allowing us to use the window decoding [4]. Since the variable nodes are separated by at least $m_{cc} + 1$ time steps, they cannot be connected to the same check node, and the window size should therefore be $W \geq m_{cc} + 1$. The window decoder at any position, t, covers the received signals, [$\mathbf{y}_t$, $\mathbf{y}_{t+1}$, ..., $\mathbf{y}_{t+W-1}$]. These received signals are decoded by computing the log-likelihood ratios (LLRs) of the variable nodes and check nodes within a window decoder. For example, in Fig. 2, the received signals, [$\mathbf{y}_t$, $\mathbf{y}_{t+1}$, $\mathbf{y}_{t+2}$, $\mathbf{y}_{t+3}$], are passed to the window decoder with $W = 4$. The received signal $\mathbf{y}_t$, will then be decoded, and hence the variable nodes involving the received signal $\mathbf{y}_t$ are known as the

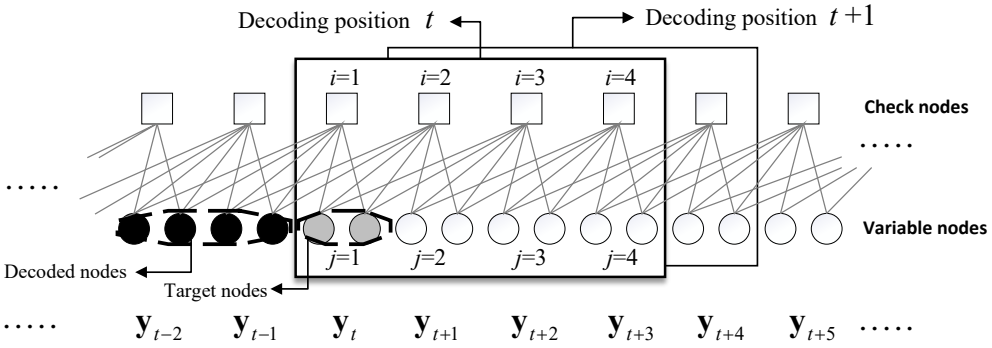

Fig. 2: *Sliding window decoding with $W = 4$, operated at positions 't' and 't+1'. The protograph structure of the SC-LDPC code is $\boldsymbol{B}_{1,t} = \boldsymbol{B}_{2,t} = \boldsymbol{B}_{3,t} = [1\ 1]$.*

$$\mathbf{B} = \begin{bmatrix} \mathbf{B}_{1,1-m_{cc}} & & & & & & & \\ \mathbf{B}_{2,1-m_{cc}} & \ddots & & & & & & \\ \vdots & \vdots & \mathbf{B}_{1,t} & & & & & \\ \mathbf{B}_{m_{cc}+1,1-m_{cc}} & \vdots & \mathbf{B}_{2,t} & \ddots & & & & \\ & \ddots & \vdots & \vdots & \mathbf{B}_{1,L+m_{cc}-2} & & & \\ & & \mathbf{B}_{m_{cc}+1,t} & \vdots & \mathbf{B}_{2,L+m_{cc}-2} & \mathbf{B}_{1,L+m_{cc}-1} & & \\ & & & \ddots & \mathbf{B}_{3,L+m_{cc}-2} & \mathbf{B}_{2,L+m_{cc}-1} & \mathbf{B}_{1,L+m_{cc}} \end{bmatrix} \tag{3}$$

"target nodes". After releasing the target nodes, the window shifts to the next position, $t = t + 1$, to decode the received signal, $\mathbf{y}_{t+1}$. According to the approximated LLR reliabilities, the window can be shifted to more than one position to reduce complexity, as suggested in our prior work [8].

Since the window decoder cannot perform well at the beginning and end of the SC-LDPC codeword, the additional variable nodes or trailing bits must be attached to a protograph of SC-LDPC codes. The number of trailing bits must be carefully selected because too many trailing bits causes a rate-loss issue in the SC-LDPC codes.

In this paper, the number of trailing bits is set to m_{cc}. Hence, the matrix, $\mathbf{B}$, of the SC-LDPC codes with trailing bits can be rewritten as shown in Eq. (3). The matrix, $\mathbf{B}$, measures $n_c(L+2m_{cc})\times n_v(L+2m_{cc})$. Hence, the code rate of the SC-LDPC codes with trailing bits is

$$R_{SC\_TB} = \left(1 - \frac{n_c}{n_v}\right)\left(\frac{1}{1 + (2m_{cc}/L)}\right). \tag{4}$$

Due to the additional trailing bits, the SC-LDPC code has a rate-loss issue, as can be observed in Eq. (4). In [14], the matrix, $\mathbf{B}$, of the SC-LDPC code is modified to handle the rate-loss issue. The method used in [14] is not considered in this paper, however, our proposed associated sectors can mitigate the rate-loss issue in a straightforward manner, as detailed in Section 4.3.

3. SC-LDPC CODES IN MAGNETIC RECORDING SYSTEMS

3.1 Channel Model

In this paper, we consider bit pattern-media magnetic recording (BPMR) systems [15], consisting of intersymbol interference (ISI) and inter-track interference (ITI). A block diagram of our system is presented in Fig. 3. On the transmitter side, the SC-LDPC encoder maps the user information, $\mathbf{u}_t = [u_{1,k}, u_{2,k}, \ldots, u_{j,k}, \ldots, u_{(n_v-n_c),k}]$ to the codeword, $\mathbf{v}_t = [v_{1,k}, v_{2,k}, \ldots, v_{j,k}, \ldots, v_{n_v,k}]$. The modulated codeword, $\mathbf{x}_t = 2\mathbf{v}_t - 1$, is then recorded on a BPMR system. It should be noted that the recording mechanism of magnetic recording systems can employ either non-associated sectors or the proposed associated sectors. Details of the non-associated and proposed associated sectors are provided in the next section. The readback, $\mathbf{r}_t = [r_{1,k}, r_{2,k}, \ldots, r_{j,k}, \ldots, r_{n_v,k}]$ of the magnetic island j, along track k, is computed by

$$r_{j,k} = \sum_{a=-A}^{A} \sum_{b=-B}^{B} h_{a,b} x_{j-a,k-b} + n_{j,k} \tag{5}$$

where $\mathbf{n}_t = [n_{1,k}, n_{2,k}, \ldots, n_{j,k}, \ldots, n_{n_v,k}]$ denoting an AWGN sequence. The fraction, $h_{a,b}$, is a two-dimensional (2-D) channel coefficient, generated by sampling the Gaussian pulse response at the multiple integers, covering $2A + 1$ bits and $2B + 1$ tracks. We consider the BPMR channel with an areal density of 2 terabits-per-square-inch (Tb/in^2), where both magnetic island periods and track pitch measure 18 nm. The half pulse widths of the along-track and across-track pulse responses are 19.4 and 24.8 nm, respectively. The 2-D channel matrix [16] is,

$$\mathbf{H}_{2\text{Tb}} = \begin{bmatrix} 0.0213 & 0.2321 & 0.0213 \\ 0.0919 & 1 & 0.0919 \\ 0.0213 & 0.2321 & 0.0213 \end{bmatrix}. \tag{6}$$

Moreover, we consider the higher areal density of 4 Tb/in^2 in which both magnetic island periods and track pitch are decreased to 12.5 nm. The half pulse widths of

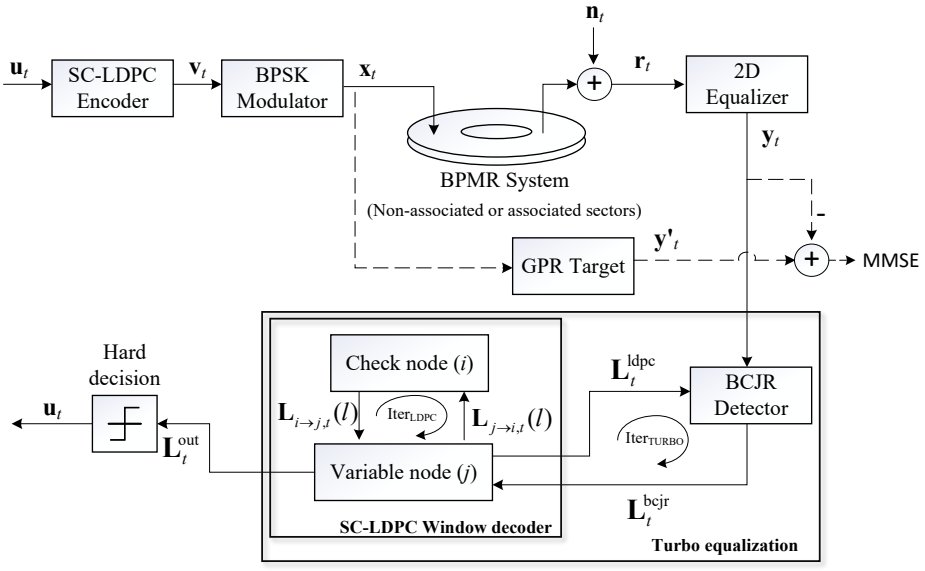

Fig. 3: *SC-LDPC codes in the BPMR system.*

the along-track and across-track pulse responses are 13.5 and 19.2 nm, respectively. The 2-D channel matrix [17] is

$$\mathbf{H}_{4\text{Tb}} = \begin{bmatrix} 0.0287 & 0.3088 & 0.0287 \\ 0.0928 & 1 & 0.0928 \\ 0.0287 & 0.3088 & 0.0287 \end{bmatrix}. \tag{7}$$

On the receiver side, the readback, $\mathbf{r}_t$, is passed to a 2D equalizer to handle the ISI and ITI effects. The 2D equalizer coefficients and the generalized partial response (GPR) target are designed to minimize the mean-squared error (MMSE) [18]. However, we focus on the single-track detection by considering only the recorded data on the main track, $k = 0$.

3.2 Turbo Equalization

High-density magnetic recording systems [6–8] always cope with impairments arising from both ISI and ITI. One technique for achieving a required BER is to use turbo equalization. In our prior work [8], turbo equalization, consisting of the BCJR detector [19] and SC-LDPC window decoder, is used to mitigate the ISI and ITI in BPMR systems. In this subsection, we briefly explain the turbo equalization scheme, starting with the BCJR detector and ending with the SC-LDPC decoder.

3.2.1 BCJR detector

The BCJR detector receives the signal, $\mathbf{y}_t, t = 1, 2, \ldots, L$ from the 2D equalizer. The BCJR algorithm [19] relies on the trellis structure (depending on the designed GPR target) and a priori LLR to compute a posteriori LLR, $\mathbf{L}_t^{bcjr}$, as described by the joint probability equation [19],

$$\begin{aligned} \mathbf{L}_t^{bcjr} &= \log \frac{\sum\limits_{U^+} p\left(s', s, \mathbf{y}_t\right)}{\sum\limits_{U^-} p\left(s', s, \mathbf{y}_t\right)} \\ &= \log \left[\frac{\sum\limits_{U^+} \beta_z(s)\, \gamma_z(s', s)\, \alpha_{z-1}(s')}{\sum\limits_{U^-} \beta_z(s)\, \gamma_z(s', s)\, \alpha_{z-1}(s')} \right] \end{aligned} \tag{8}$$

where $p\left(s', s, \mathbf{y}_t\right)$ is the joint probability of receiving the sequence $\mathbf{y}_t$, and being in state s' at trellis section $z-1$, and state s at the current trellis section z. The summation of all state transitions from s' to s, caused by transmitted bits $x_z = +1$ and -1 is computed using U^+ and U^-, respectively. The value, $\alpha_{z-1}(s')$, defines the forward state probability

$$\alpha_z(s) = \sum_{s'} \gamma_z(s', s)\, \alpha_{z-1}(s') \tag{9}$$

where the recursion for $\alpha_z(s)$ is initialized according to $\alpha_0(s) = 1$ if $s = 0$ and $\alpha_0(s) = 0$ if $s \neq 0$. Moreover, the value, $\beta_z(s)$, defines the backward state probability,

$$\beta_{z-1}(s') = \sum_{s} \beta_z(s)\, \gamma_z(s', s) \tag{10}$$

where the recursion for $\beta_{z-1}(s')$ is initialized according to $\beta_z(s) = 1$ if $s = 0$ and $\beta_z(s) = 0$ if $s \neq 0$. Both the values, $\alpha_{z-1}(s')$ and $\beta_z(s)$, are computed recursively across the trellis section. The branch metrics or trellis path transition probabilities are referred to as $\gamma_z(s', s)$, determined for the trellis section z and $z-1$ as given in [19],

$$\gamma_z(s', s) = \frac{P(x_z)}{2\pi\sigma^2} \exp\left(-\frac{(y_z - x_z)^2}{2\sigma^2} \right) \tag{11}$$

where $P(x_z)$ is the a priori probability, which is computed using the a priori LLR, L_z^{ldpc}, from the SC-LDPC decoder [19]. The value, σ^2, is the variance of AWGN sequence. Finally, the BCJR detector computes the posteriori LLRs, $\mathbf{L}_t^{bcjr}$, $t = 1, 2, \ldots, L$, via Eq. (8) using Eqs. (9), (10), and (11); then sends them to the SC-LDPC decoder.

3.2.2 SC-LDPC window decoder

As described in Section 2.2, SC-LDPC decoding is performed by sliding a window decoder along the sequential variable node position, t. At any position, t, $\mathbf{L}_{j\to i,t}(l)$ can be defined as the LLR from the variable node j to check node i at decoding iteration l.

$$\mathbf{L}_{j\to i,t}(l) = \mathbf{L}_{j,t}^{bcjr} + \sum_{i'\in N(j)\backslash i} \mathbf{L}_{i'\to j,t}(l-1) \tag{12}$$

where $\mathbf{L}_{j,t}^{bcjr}$ defines the posteriori LLR of the BCJR detector sent to the variable node j at position t. If $l = 1$, $\mathbf{L}_{i'\to j,t}(l-1)$. Similarly,$\mathbf{L}_{i\to j,t}(l)$ is the LLR from the check node i to variable node j at decoding iteration, l

$$\mathbf{L}_{i\to j,t}(l) = 2\tanh^{-1}\left(\prod_{j'\in N(i)\backslash j} \tanh\left(\frac{\mathbf{L}_{j'\to i,t}(l)}{2}\right)\right) \tag{13}$$

where $1 \le i, j \le W$ and $1 \le l \le \mathrm{Iter}_{\mathrm{LDPC}}$. $N(j)\backslash i$ is the set of check nodes connected to the variable node j, excluding the check node i, while $N(i)\backslash j$ is the set of variable nodes connected to the check node i, excluding variable node j. The LLRs of variable nodes and check nodes within a window are produced following Eqs. (12)–(13), until the maximum number of decoding iterations, $\mathrm{Iter}_{\mathrm{LDPC}}$, is reached. Then the LLR, $\mathbf{L}_t^{ldpc}$, of the target variable node is computed by

$$\mathbf{L}_t^{ldpc} = \sum_{i\in N(1)} \mathbf{L}_{i\to 1,t}(\mathrm{Iter}_{\mathrm{LDPC}}) \tag{14}$$

where $N(1)$ is the set of check nodes connected to the first variable node. After computing Eq. (14), the window moves to the next position, $t = t + 1$. The decoding in Eqs. (12)–(14) is repeated until it reaches $t = L$. Then the SC-LDPC decoder sends all output (a priori) LLRs, $\mathbf{L}_t^{ldpc}$, $t = 1, 2, \ldots, L$, to update the branch metric, γ, of the BCJR detector. The same process continues until the maximum number of turbo iterations, $\mathrm{Iter}_{\mathrm{TURBO}}$, is reached. Then all user information, $\mathbf{u}_t$, is decided based on the output LLR

$$\mathbf{L}_t^{out} = \mathbf{L}_{1,t}^{bcjr} + \sum_{i\in N(1)} \mathbf{L}_{i\to 1,t}(\mathrm{Iter}_{\mathrm{LDPC}}) \tag{15}$$

where $\mathbf{L}_{1,t}^{bcjr}$ is a posteriori LLR of the BCJR detector sent to the first variable node at position t.

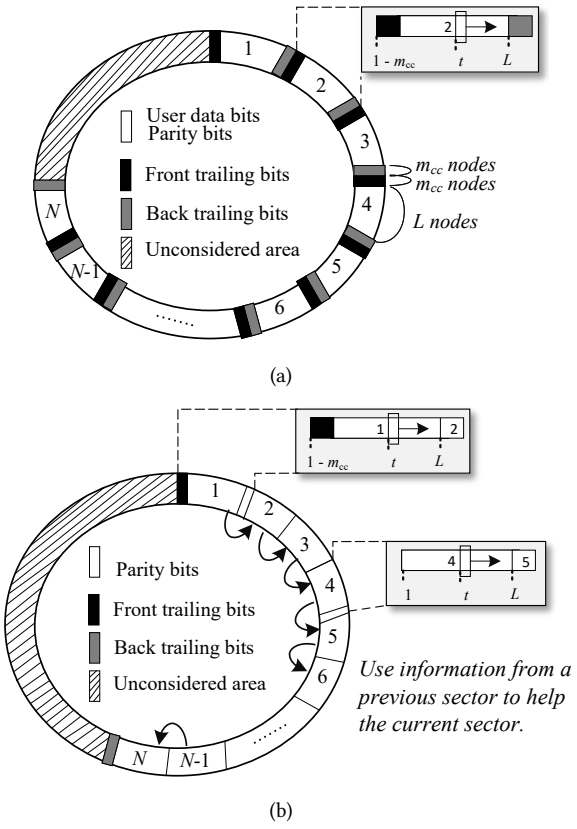

Fig. 4: *Illustration of (a) non-associated sectors and (b) associated sectors.*

4. ASSOCIATED SECTORS OF MAGNETIC RECORDING SYSTEMS VIA SC-LDPC CODES

4.1 Non-Associated Sectors vs. Associated Sectors

For the traditional magnetic recording system [6–8], the entire user bits are divided into N blocks. Each block is then encoded and recorded on N consecutive sectors. Since there is no edge connection between the variable nodes in consecutive sectors, they are denoted as non-associated sectors. After adding the trailing bits to the front and back of SC-LDPC codewords, the additional variable nodes or trailing bits then appear in every sector, as illustrated in Fig. 4(a). It should be noted that the front trailing bits must be '0' or known bits while the back trailing bits can be arbitrary or unknown. In any sector, the window decoder starts to decode from position $t = 1 - m_{cc}$ to L. The code rates of the SC-LDPC in non-associated sectors can be written as

$$R_{NA} = R_{SC\_TB} = \left(1 - \frac{n_c}{n_v}\right)\left(\frac{1}{1 + \left(\frac{2m_{cc}}{L}\right)}\right). \tag{16}$$

In the non-associated sectors, the previous sectors cannot be used to reinforce the decoding to retrieve the data bits in the current sector. Therefore, the associated sectors generated by the SC-LDPC codes are proposed for the BPMR system. The associated sectors are illustrated

in Fig. 4(b). The entire user bits are encoded continuously to obtain a single codeword. The codeword is then divided and recorded in consecutive N sectors. The front trailing bits are placed in the first sector, and the back trailing bits in the N^{th} sector. This process is used to construct the associated sectors using the SC-LDPC code structure to connect the codewords in a chain, resulting in edge connections between two adjacent sectors.

4.2 Reading Mechanism of Associated Sectors

Although a single codeword appears to be stored in consecutive N sectors, the window decoder can operate on any n^{th} sector. The window decoder starts to decode from position $t = 1 - m_{cc}$ to L for the first sector and $t = 1$ to L for the other sectors where $n > 1$. The benefit of combining the recording process with the associated sectors is that when the decoder can no longer correct the erroneous bits in the n^{th} sector, it will decode a portion of the $(n-1)^{\text{th}}$ sector to obtain new LLRs. The cooperation between two adjacent sectors is straightforward: after decoding at the n^{th} sector is completed and erroneous bits remain, the window decoder is placed at the $(n-1)^{\text{th}}$ sector. The window decoder subsequently moves along the variable nodes, and the new LLRs from the $(n-1)^{\text{th}}$ sector will be delivered along with it. As soon as the window arrives at the n^{th} sector, the new LLRs from the $(n-1)^{\text{th}}$ sector will be used to compute the LLRs of the n^{th} sector. The remaining erroneous bits in the n^{th} sector may or may not be corrected, depending on the level of LLR reliability coming from the $(n-1)^{\text{th}}$ sector.

The disadvantage of associated sectors is that when the window decoder operates at time $t = L$ in the n^{th} sector, the first m_{cc} variable nodes of the $(n+1)^{\text{th}}$ sector must be included in the window decoder. Moreover, when the n^{th} sector is rewritten, the $(n+1)^{\text{th}}$ to N^{th} sectors must also be rewritten.

4.3 Code-Rate Tendencies and Rate-Loss Mitigation

Since the trailing bits appear in the first sector and N^{th} sectors, the code rate of the SC-LDPC in the associated sectors can be computed by

$$R_A = \left(1 - \frac{n_c}{n_v}\right)\left(\frac{1}{1 + \left(\frac{2m_{cc}}{(N \cdot L)}\right)}\right). \tag{17}$$

From Eq. (17), it can be observed that associated sectors can mitigate the rate-loss issue when (N) is very large. Fig. 5 shows the code rates of the SC-LDPC recorded in non-associated and associated sectors for any number of sectors (N). Given that the SC-LDPC code is constructed by $\mathbf{B}_{1,t} = \mathbf{B}_{2,t} = \mathbf{B}_{3,t} = [1\ 1\ 1\ 1\ 1\ 1\ 1\ 1\ 1]$, $m_{cc} = 2$, and $L = 100$, the original code rate without trailing bits (R_{SC}) is 0.8889 (indicated by a solid line). When the SC-LDPC code is recorded using the traditional non-associated sector method, the code rate (R_{NA}) loss

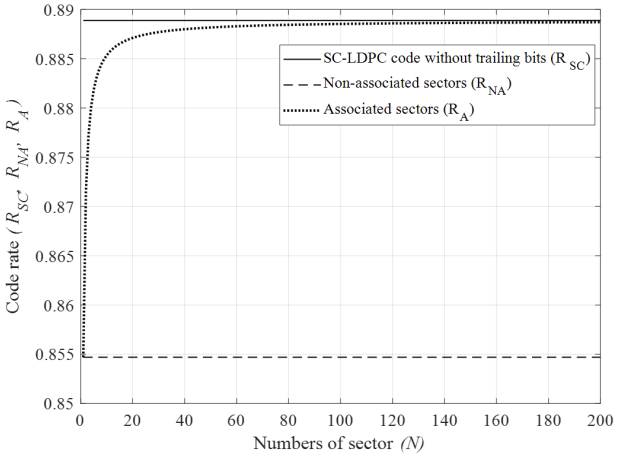

Fig. 5: *Code rates of the SC-LDPC in non-associated and associated sectors.*

is 0.8547 (indicated by a dashed line). In the associated sectors, the code rate (R_A) increases with N and reaches the original code rate at a large N (indicated by a dotted line). As a result, the associated sectors can reduce the rate-loss issue of SC-LDPC codes at large N. In Section 4.4, the theoretical tool, i.e., the P-EXIT chart [10] is used to evaluate the performance of SC-LDPC codes recorded in the non-associated and associated sectors.

4.4 P-EXIT Chart Analysis

In this section, we present a theoretical analysis of SC-LDPC codes in non-associated and associated sectors by modifying the P-EXIT chart [10]. The P-EXIT chart is a technique for tracking mutual information between the LLRs along the edges of the protograph and coded bits. During iterative decoding between the BCJR detector and SC-LDPC decoder, mutual information is produced and exchanged. Let I^{Ed} be the mutual information output of the BCJR detector at any n^{th} sector. Unfortunately, since I^{Ed} cannot be calculated in the close form equation, the Monte Carlo simulation [20] is used to estimate I^{Ed}. Given that the code rate (R), signal-to-noise ratio (E_b/N_0), and mutual information input of the BCJR detector are known, the experimental $I^{Ed}(r)$, produced at the turbo iteration r, can be computed by

$$I^{Ed}(r) = 1 - \mathrm{E}\left[\log_2\left(1 + \exp\left(-\mathbf{L}_t^{bcjr}\right)\right)\right] \tag{18}$$

where $1 \le r \le \mathrm{Iter}_{\mathrm{TURBO}}$, $\mathrm{E}[\cdot]$ is the expected operation, and $\mathbf{L}_t^{bcjr}$ is the output (a posteriori) LLR of the BCJR detector at position t.

To compute the mutual information in the window decoder, the indices i are defined as the position of check node and indices j, as the position of the variable node within a window at position t. In addition, the element b_{ij} is defined as the number of protograph edges between the check node i and variable node j. The mutual information $I^{Ev}_{j\to i,t}(l)$, produced from the variable node j to the check node i at the decoding iteration l, can be computed by

$$I_{j\to i,t}^{Ev}(l) = J\left(\left\{\sum_{c=1}^{W}\left\{(b_{cj}-\tau)\left[J^{-1}\left(I_{c\to j,t}^{Ec}(l-1)\right)\right]^2 + \left(J^{-1}\left(I^{Ed}(r)\right)\right]^2\right\}\right\}^{\frac{1}{2}}\right) \quad (19)$$

where $1 \le l \le \text{Iter}_{\text{LDPC}}$, $\tau = 1$ if $c = i$ and $\tau = 0$ if $c \ne i$. The polynomial approximations of function $J(\cdot)$ and its inverse function $J^{-1}(\cdot)$ are given in [21]. Similarly, the counterpart mutual information $I_{i\to j,t}^{Ec}(l)$ from the check node i to the variable node j can be computed as

$$I_{i\to j,t}^{Ec}(l) = 1 - J\left(\left\{\sum_{c=1}^{W}\left\{(b_{ic}-\tau)\left[J^{-1}\left(1-I_{c\to i,t}^{Ev}(l)\right)\right]^2\right\} + \sum_{k=1}^{m_{cc}}\left\{b_{i+k,1}\left[J^{-1}\left(1-I_{1\to i+k,t-k}^{Ev}(\text{Iter}_{\text{LDPC}})\right)\right]^2\right\}\right\}^{\frac{1}{2}}\right) \quad (20)$$

where $\tau = 1$ if $c = j$ and $\tau = 0$ if $c \ne j$.

Recording mechanisms such as the non-associated and associated sectors have an impact on the use of Eq. (20). For the non-associated sectors (or associated sectors at $n = 1$), the mutual information, $I_{c\to i,t}^{Ev}(l)$, of the front trailing bit, where $1 - m_{cc} \le t \le 0$ and $1 \le c \le 1 - t$, must be 1. On the other hand, in the case of associated sectors at $n > 1$, we will assign $I_{c\to i,t}^{Ev}(l) = 0$ for the edges connecting variable nodes outside the sectors. This is because no information is passed along these edges. In the case of associated sectors with assistance from a previous sector, $I_{c\to i,t}^{Ev}(l)$ exists between 0 and 1 since the edges contain the information sent from the previous sector. The mutual information calculations in Eqs. (19)–(20) are repeated for $\text{Iter}_{\text{LDPC}}$. The cumulative mutual information $I_{j,t}^{Cm}$, and a priori mutual information $I_{j,t}^{Ad}$, of each variable node can then be computed by

$$I_{j,t}^{Cm} = J\left(\left\{\sum_{i=1}^{W}\left\{b_{ij}\left[J^{-1}\left(I_{i\to j,t}^{Ec}(\text{Iter}_{\text{LDPC}})\right)\right]^2 + \left[J^{-1}\left(I^{Ed}(r)\right)\right]^2\right\}\right\}^{\frac{1}{2}}\right) \quad (21)$$

and

$$I_{j,t}^{Ad} = J\left(\left\{\sum_{i=1}^{W}\left\{b_{ij}\left[J^{-1}\left(I_{i\to j,t}^{Ec}(\text{Iter}_{\text{LDPC}})\right)\right]^2\right\}\right\}^{\frac{1}{2}}\right). \quad (22)$$

Following the computation of Eqs. (21) and (22), the window shifts to the next decoding position $t = t + 1$ until $t = L$. Afterward, the mutual information input of the BCJR detector will be estimated by averaging a priori mutual information, $I_{1,t}^{Ad}$, as

$$I^{Ad}(r) = \frac{1}{L}\sum_{t=1}^{L} I_{1,t}^{Ad}. \quad (23)$$

For the next turbo iteration $r = r + 1$, $I^{Ed}(r)$ in Eq. (18) will be reinitialized by the incoming $I^{Ad}(r-1)$. The mutual information calculations in Eqs. (18)–(23) will be repeated for $\text{Iter}_{\text{TURBO}}$. Finally, the average cumulative mutual information of the target node, I_{target}^{Cm}, is used to present the mutual information window decoder output:

$$I_{target}^{Cm} = \frac{1}{L}\sum_{t=1}^{L} I_{1,t}^{Cm}. \quad (24)$$

The theoretical performance of SC-LDPC codes recorded in the non-associated and associated sectors are evaluated according to the *decoding threshold*, which is the lowest E_b/N_0 (dB) for which $I_{target}^{Cm} \to 1$. The decoding threshold is the lowest channel quality, allowing for reliable iterative decoding of SC-LDPC codes.

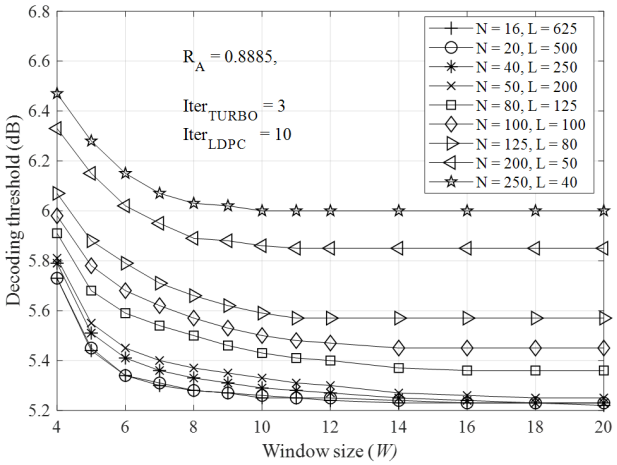

Fig. 6: *Decoding thresholds of associated sectors with a fixed code rate, where the window decoder does not use information from the previous sector.*

5. THEORETICAL RESULTS

5.1 Associated Sectors with and without Previous Sector Information

Fig. 6 shows the decoding threshold tendencies of associated sectors, generated by the SC-LDPC code with $\mathbf{B}_{1,t} = \mathbf{B}_{2,t} = \mathbf{B}_{3,t} = [1\ 1\ 1\ 1\ 1\ 1\ 1\ 1\ 1]$ and $m_{cc} = 2$. We set $\text{Iter}_{\text{TURBO}} = 3$ and $\text{Iter}_{\text{LDPC}} = 10$. In this analysis, we consider the BPMR system with areal density of 2 Tb/in^2, with the 2-D channel matrix given in Eq. (6). Our results show that the decoding thresholds decrease (improve) when the window size (W) increases and stops decreasing at $W \ge 12$. Here, we fix $R_A = 0.8885$, and hence the parameters N and L in Eq. (17) can be varied. The decoding thresholds are decreased by increasing the coupling length (L) (or sector size) and

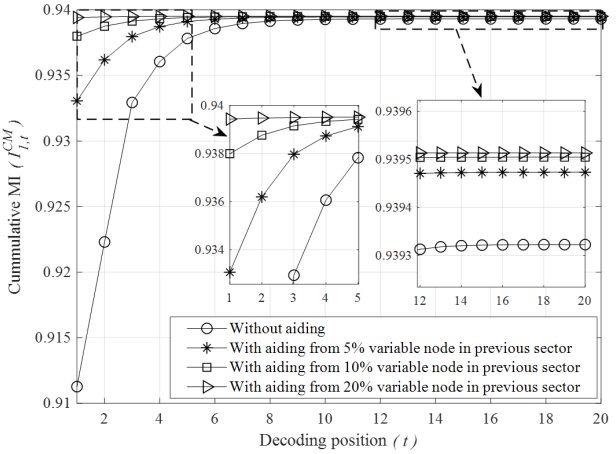

Fig. 7: *Mutual information on associated sectors, where the window decoder uses information from the previous sector. The signal-to-noise ratio, $E_b/N_0 = 5$ dB.*

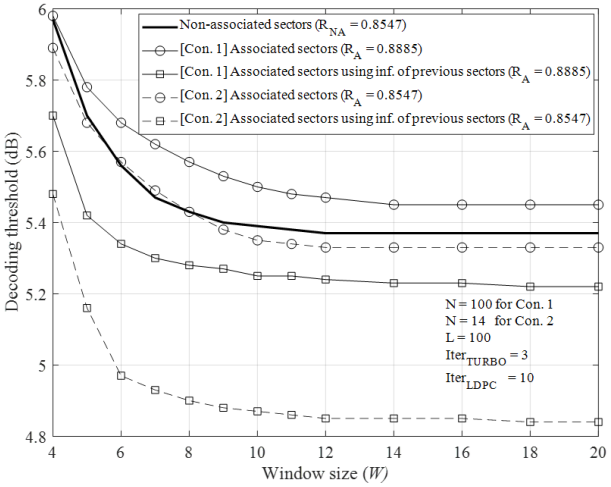

Fig. 9: *Decoding threshold of SC-LDPC codes in the BPMR system with an areal density of 2 Tb/in^2.*

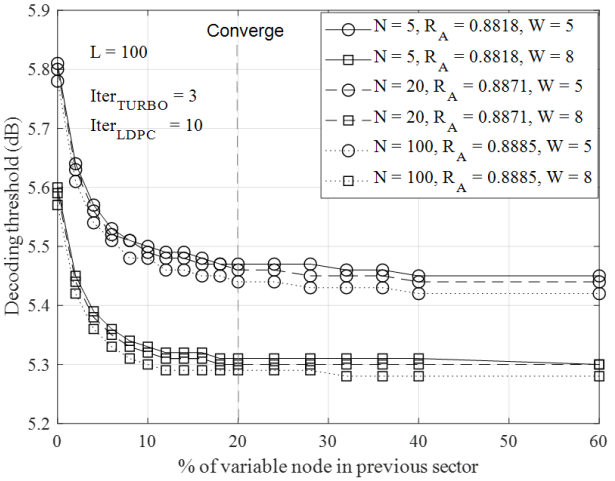

Fig. 8: *Decoding thresholds of associated sectors, where the window decoder uses information from the previous sector.*

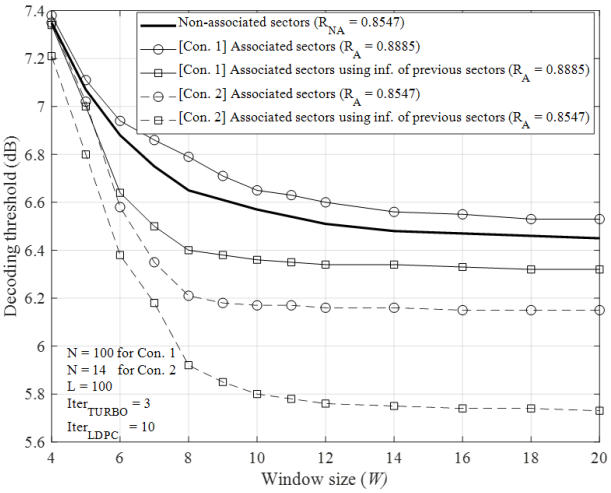

Fig. 10: *Decoding threshold of SC-LDPC codes in BPMR system with an areal density of 4 Tb/in^2.*

decreasing the number of sectors (N). Specifically, the decoding thresholds stop decreasing when $N = 20$ and $L = 500$.

Fig. 7 shows the cumulative mutual information of the target node $I_{1,t}^{Cm}$ in Eq. (21) for the SC-LDPC codes in the associated sectors. The window size (W) is fixed to 8. The theoretical analysis shows that $I_{1,t}^{Cm}$ increases with the decoding position (t) and saturates at the decoding position $t > 10$. This is due to the fact that $I_{1,t}^{Cm}$ continually accumulates when the window decoder moves from $t = 1$ to L. When the information (5, 10, and 20% variable nodes) from a previous sector is requested, $I_{1,t}^{Cm}$ improves, especially in the early decoding positions.

The decoding thresholds of associated sectors are shown in Fig. 8, whereby information from the previous sectors is requested to reinforce the decoding of the current sector. When the variable nodes from the previous sector are used to decode the current sector, the decoding thresholds decrease. The decoding thresholds stop decreasing when 20% of variable nodes in the previous sector are used. The decoding thresholds are decreased (improved) by ~0.35 dB for $W = 5$ and ~0.3 dB for $W = 8$. Furthermore, the decoding thresholds are also shown to decrease when N is increased. This is because a large N can offset the performance degradation caused by the SC-LDPC code rate-loss issue.

5.2 Non-Associated Sectors vs. Associated Sectors

Fig. 9 presents a comparison of the decoding thresholds for the non-associated and associated sectors under the two different conditions.

- In the first condition (Con. 1, indicated by solid lines with a symbol), we compare the decoding thresholds of the same protograph structure, where $\mathbf{B}_{1,t} = \mathbf{B}_{2,t} = \mathbf{B}_{3,t} = [1\ 1\ 1\ 1\ 1\ 1\ 1\ 1\ 1]$, $m_{cc} = 2$, $L = 100$, and $N = 100$. Thus, the code rate for non-associated sectors is $R_{NA} = 0.8547$, and associated sectors $R_A = 0.8885$. The non-associated sectors have lower (better) decoding thresholds than the associated sectors. However, when

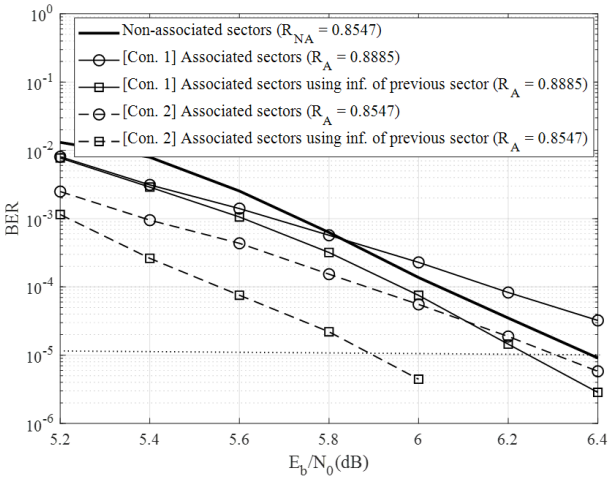

Fig. 11: BERs of SC-LDPC codes in the BPMR system with an areal density of 2 Tb/in^2.

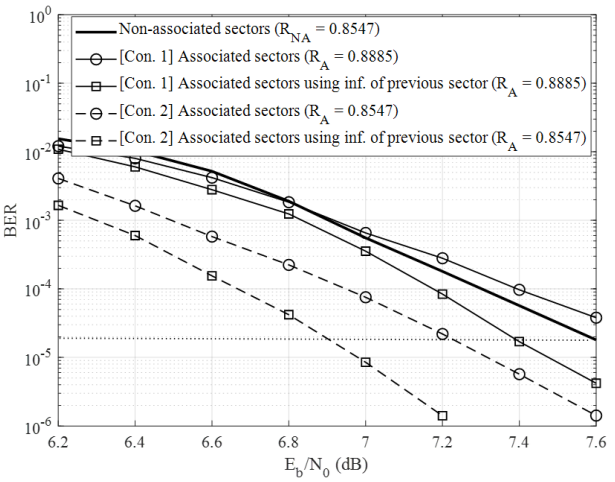

Fig. 12: BERs of SC-LDPC codes in the BPMR system with an areal density of 4 Tb/in^2.

information from the previous sector is requested, the decoding thresholds of associated sectors are lower than those of non-associated sectors by ~0.18 dB with a window size $W \geq 8$.

- In the second condition (Con. 2, indicated by dashed lines), we compare the decoding thresholds at the same code rate, namely $R_{NA} = R_A = 0.8547$. It should be noted that the SC-LDPC code for the associated sectors is reconstructed by $\mathbf{B}_{1,t} = \mathbf{B}_{2,t} = \mathbf{B}_{3,t} = [1\ 1\ 1\ 1\ 1\ 1]$. We set $L = 100$ and $N = 14$ to obtain $R_A = 0.8547$. The results show that the decoding thresholds of associated sectors are much lower (better) than those of non-associated sectors when information from the previous sector is requested. The decoding thresholds are reduced by ~0.5 dB compared to the non-associated sectors at $W \geq 8$, implying the clear benefits of receiving aid from the previous sector.

For the higher areal density of 4 Tb/in^2 (2-D channel matrix is given in Eq. (7)), the decoding threshold comparison is presented in Fig. 10. When the information from the previous sector is requested, the decoding thresholds of associated sectors improve; as a result, they have a lower (better) decoding threshold than the traditional non-associated sectors. Compared to the non-associated sectors at $W \geq 8$, Con. 1 has a reduced decoding threshold of ~0.2 dB, while Con. 2 has a reduced decoding threshold of ~0.7 dB.

Although the P-EXIT chart is a theoretical analysis tool, the decoding thresholds determined by the P-EXIT chart are reasonably consistent with the waterfall-region performance of the simulated BER as shown in Section 6.

6. COMPUTER-BASED SIMULATION RESULTS

In this section, computer simulations are used to validate the theoretical results of non-associated and associated sectors produced from the P-EXIT chart. In our simulations, the parity-check matrix $\mathbf{H}_t$ is constructed from the progressive edge-growth algorithm [22] with an expansion factor of $M = 30$.

6.1 Non-Associated Sectors vs. Associated Sectors

The simulation results in Fig. 11 back up our theoretical results in Fig. 9 for the areal density of 2 Tb/in^2. The BERs of the SC-LDPC codes with associated sectors are worse than those of non-associated sectors for the same protograph structure (Con. 1, indicated by solid lines with a symbol). Fortunately, our associated sectors can request 20% of new LLRs from the previous sector to improve the decoding performance of the current sector when decoding failure (remaining erroneous bits) is encountered. In this paper, we use the results from the parity-check equation, as introduced for the SC-LDPC window decoder by Kang *et al.* [23], to detect erroneous bits in any sector. As a result, the BERs of SC-LDPC codes with associated sectors are improved when information from the previous sector is requested. Therefore, the associated sectors have superior BERs, which provide a ~0.18 dB coding gain compared to the non-associated sectors with a BER of 1×10^{-5}. At the same code rate (Con. 2, indicated by dashed lines), the coding gain of associated sectors increases to ~0.5 dB.

For the BPMR system with a higher areal density of 4 Tb/in^2, the simulation results in Fig. 12 corroborate our theoretical results in Fig. 10, demonstrating that the associated sectors still outperform the non-associated sectors. At a BER of 2×10^{-5}, the achieved coding gain is ~0.2 dB for Con. 1 and ~0.7 dB for Con. 2. Furthermore, Fig. 12 implies that we can achieve greater coding advantages when the associated sectors are used in a BPMR system at a higher areal density.

6.2 Full Block Decoding vs. Window Decoding

For all contributions in this paper, we used a window decoding approach to decode the associated sectors, whereby the previous sector can be reread to correct erroneous bits in the current sector. However, Lentmaier *et al.* showed that window decoding reduces decoding complexity and latency at the cost of BER deterioration

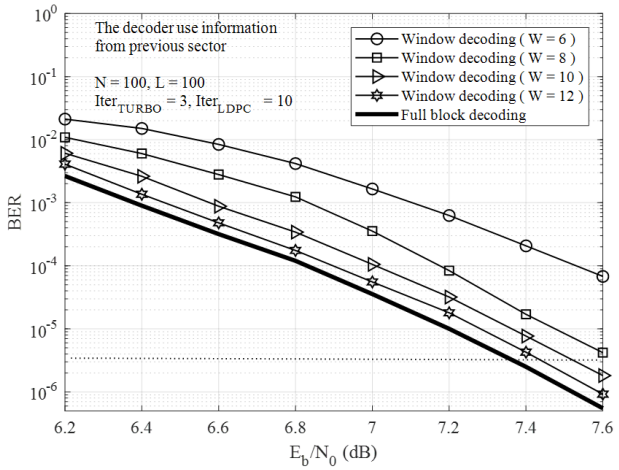

Fig. 13: BERs of the full block and window decoding in the BPMR system with an areal density of 4 Tb/in^2.

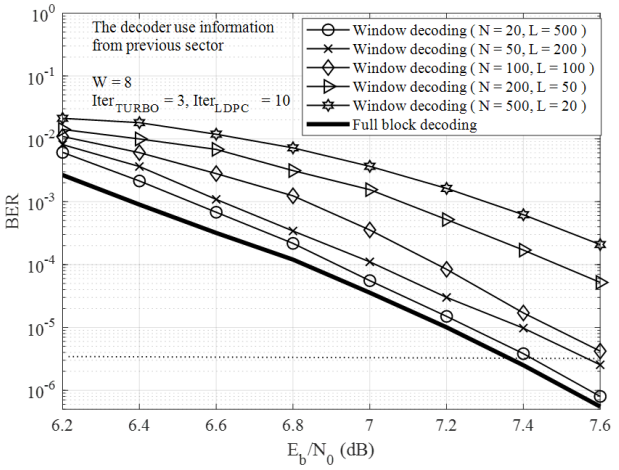

Fig. 14: BERs for fixed $W = 8$ of the full block and window decoding in the BPMR system with an areal density of 4 Tb/in^2.

when compared to full (entire) block decoding [24]. Therefore, in this paper, we compare the BERs of associated sectors, decoded using full block and window decoding for a more comprehensive examination.

We consider only Con. 1, where the SC-LDPC codes are constructed by $\mathbf{B}_{1,t} = \mathbf{B}_{2,t} = \mathbf{B}_{3,t} = [1\ 1\ 1\ 1\ 1\ 1\ 1\ 1]$, $m_{cc} = 2$, $L = 100$, and $N = 100$. The window size W ranges from 6 to 12. The results in Fig. 13 demonstrate that BERs improve as the window size W, increases, but they are also less effective than full block decoding. At a BER of 3×10^{-6}, we lose many gains for small $W = 6$. For the larger $W = 8$ and 10, we lose gains of ~0.22 dB and ~0.12 dB, respectively. In particular, for the largest $W = 12$, we lose the slight gain of ~0.05 dB compared to full block decoding.

In Fig. 14, the BERs are exhibited for fixed $W = 8$, while the parameters N and L in Eq. (17) vary. The simulation results back up our theoretical results in Fig. 6, indicating that increasing L (or decreasing N) improves the BERs. Here, we can achieve the best possible BER by using $N = 20$ and $L = 500$, which loses only a ~0.03 dB gain when compared to full block decoding.

7. CONCLUSION

In this paper, we propose the construction of associated sectors via SC-LDPC codes. When the decoder fails to retrieve the data stored in the current sector, it can request information from the previous sector to aid the decoding of the current sector. We analyze the decoding thresholds of associated sectors by applying the P-EXIT chart. The associated sectors offer lower decoding thresholds than the non-associated sectors. Our theoretical results are confirmed by computer simulation. In the BPMR system with 2 Tb/in^2, the associated sectors can give ~0.18 and ~0.5 dB coding gains compared to the non-associated sectors of the same protograph structure (Con. 1) and code rate (Con. 2), respectively. At a higher areal density of 4 Tb/in^2, the associated sectors still outperform the non-associated sectors. The coding gains increase to ~0.2 dB for Con. 1, and ~0.7 dB for Con. 2.

Based on our theoretical results and computer-based simulation results, the associated sectors tend to be a better option for applying SC-LDPC codes in ultra-high-density data storage systems.

ACKNOWLEDGMENT

This work was supported in part by the Thailand Research Fund (TRF) and Seagate Technology (Thailand) through the Research and Researchers for Industries (RRI) under Grant PHD61I0039.

REFERENCES

[1] A. Jimenez Felstrom and K. S. Zigangirov, "Time-varying periodic convolutional codes with low-density parity-check matrix," *IEEE Transactions on Information Theory*, vol. 45, no. 6, pp. 2181–2191, Sep. 1999.

[2] M. Lentmaier, A. Sridharan, D. J. Costello, and K. S. Zigangirov, "Iterative decoding threshold analysis for LDPC convolutional codes," *IEEE Transactions on Information Theory*, vol. 56, no. 10, pp. 5274–5289, Oct. 2010.

[3] S. Kudekar, T. J. Richardson, and R. L. Urbanke, "Threshold saturation via spatial coupling: why convolutional LDPC ensembles perform so well over the BEC," *IEEE Transactions on Information Theory*, vol. 57, no. 2, pp. 803–834, Feb. 2011.

[4] A. R. Iyengar, M. Papaleo, P. H. Siegel, J. K. Wolf, A. Vanelli-Coralli, and G. E. Corazza, "Windowed decoding of protograph-based LDPC convolutional codes over erasure channels," *IEEE Transactions on Information Theory*, vol. 58, no. 4, pp. 2303–2320, Apr. 2012.

[5] A. R. Iyengar, P. H. Siegel, R. L. Urbanke, and J. K. Wolf, "Windowed decoding of spatially coupled

codes," *IEEE Transactions on Information Theory*, vol. 59, no. 4, pp. 2277–2292, Apr. 2013.

[6] H. Esfahanizadeh, A. Hareedy, and L. Dolecek, "Spatially coupled codes optimized for magnetic recording applications," *IEEE Transactions on Magnetics*, vol. 53, no. 2, Feb. 2017, Art. no. 3100211.

[7] Z. Yang, Y. Fang, G. Zhang, G. Han, and L. Kong, "Performance analysis and optimization of spatially coupled protograph-based low-density parity-check codes for two-dimensional magnetic recording systems," *IEEE Transactions on Magnetics*, vol. 56, no. 3, Mar. 2020, Art. no. 6701807.

[8] S. Khittiwitchayakul, W. Phakphisut, and P. Supnithi, "Reduced complexity window decoding of spatially coupled LDPC codes for magnetic recording systems," *IEEE Transactions on Magnetics*, vol. 54, no. 11, Nov. 2018, Art. no. 9401205.

[9] H. Esfahanizadeh, A. Hareedy, R. Wu, R. Galbraith, and L. Dolecek, "Spatially-coupled codes for channels with SNR variation," *IEEE Transactions on Magnetics*, vol. 54, no. 11, Nov. 2018, Art. no. 9401505.

[10] G. Liva and M. Chiani, "Protograph LDPC codes design based on EXIT analysis," in *IEEE GLOBECOM 2007 - IEEE Global Telecommunications Conference*, Washington, DC, USA, 2007, pp. 3250–3254.

[11] S. Khittiwitchayakul, P. Supnithi, and W. Phakphisut, "Associated sectors of magnetic recording system via spatially coupled LDPC codes," in *2021 18th International Conference on Electrical Engineering/Electronics, Computer, Telecommunications and Information Technology (ECTI-CON)*, 2021, pp. 612–615.

[12] J. Thorpe, "Low-density parity-check (LDPC) codes constructed from protographs," The Interplanetary Network Progress Report, vol. 42-154, pp. 1–7, Aug. 2003. [Online]. Available: https://ipnpr.jpl.nasa.gov/progress_report/42-154/154C.pdf

[13] D. G. M. Mitchell, M. Lentmaier, and D. J. Costello, "Spatially coupled LDPC codes constructed from protographs," *IEEE Transactions on Information Theory*, vol. 61, no. 9, pp. 4866–4889, Sep. 2015.

[14] H.-Y. Kwak, D.-Y. Yun, and J.-S. No, "Rate-loss mitigation of SC-LDPC codes without performance degradation," *IEEE Transactions on Communications*, vol. 68, no. 1, pp. 55–65, Jan. 2020.

[15] S. Nabavi, B. V. K. V. Kumar, and J. A. Bain, "Two-dimensional pulse response and media noise modeling for bit-patterned media," *IEEE Transactions on Magnetics*, vol. 44, no. 11, pp. 3789–3792, Nov. 2008.

[16] T. Sopon, P. Supnithi, and K. Vichienchom, "Improved 2-D graph-based detectors for 2-D interference channels," *IEEE Transactions on Magnetics*, vol. 50, no. 11, Nov. 2014, Art. no. 3101704.

[17] T. Sopon, L. M. M. Myint, P. Supnithi, and K. Vichienchom, "Modified graph-based detection methods for two-dimensional interference channels," *IEEE Transactions on Magnetics*, vol. 48, no. 11, pp. 4618–4621, Nov. 2012.

[18] S. Nabavi and B. V. K. V. Kumar, "Two-dimensional generalized partial response equalizer for bit-patterned media," in *2007 IEEE International Conference on Communications (ICC)*, 2007, pp. 6249–6254.

[19] W. E. Ryan and S. Lin, *Channel codes: classical and modern*. Cambridge, UK: Cambridge University Press, 2009.

[20] T. V. Nguyen, A. Nosratinia, and D. Divsalar, "Protograph-based LDPC codes for partial response channels," in *2012 IEEE International Conference on Communications (ICC)*, 2012, pp. 2166–2170.

[21] S. ten Brink, G. Kramer, and A. Ashikhmin, "Design of low-density parity-check codes for modulation and detection," *IEEE Transactions on Communications*, vol. 52, no. 4, pp. 670–678, Apr. 2004.

[22] X.-Y. Hu, E. Eleftheriou, and D. M. Arnold, "Regular and irregular progressive edge-growth tanner graphs," *IEEE Transactions on Information Theory*, vol. 51, no. 1, pp. 386–398, Jan. 2005.

[23] P. Kang, Y. Xie, L. Yang, and J. Yuan, "Reliability-based windowed decoding for spatially coupled LDPC codes," *IEEE Communications Letters*, vol. 22, no. 7, pp. 1322–1325, Jul. 2018.

[24] M. Lentmaier, M. M. Prenda, and G. P. Fettweis, "Efficient message passing scheduling for terminated LDPC convolutional codes," in *2011 IEEE International Symposium on Information Theory*, 2011, pp. 1826–1830.

Sirawit Khittiwitchayakul received the B.Eng. and M.Eng. degrees in Telecommunication Engineering from the King Mongkut's Institute of Technology Ladkrabang (KMITL), Bangkok, Thailand, in 2014 and 2017, respectively. He is currently pursuing his D.Eng. degree in Electrical Engineering at KMITL, Bangkok, Thailand. His research interests include channel coding for data storage and wireless communication technologies.

Watid Phakphisut received the B.Eng. degree in Telecommunication Engineering, the M.Eng. degree in Data Storage Technology, and the D.Eng. degree in Electrical Engineering from the King Mongkut's Institute of Technology Ladkrabang, Bangkok, Thailand, in 2009, 2011, and 2015, respectively. His research interests include the channel coding, and artificial intelligence for communication and storage systems.

Pornchai Supnithi received the B.S. degree from the University of Rochester, Rochester, NY, USA, in 1995, the M.S. degree from the University of Southern California, Los Angeles, CA, USA, in 1997 and the Ph.D. degree in Electrical Engineering from the Georgia Institute of Technology, Atlanta, GA, USA, in 2002. He is currently a full professor at Telecommunication Engineering Department, School of Engineering, King Mongkut's Institute of Technology Ladkrabang, Bangkok, Thailand. His research interests are in the area of Telecommunications, Ionospheric and GNSS, Data storage and Engineering Education. His laboratory is maintaining 7 observation stations in Thailand (with ionosonde, beacon receivers, magnetometer, and GNSS receivers) as well as Thai GNSS and Space Weather Information website. He has published over 60 journal articles with impact factors, 100 conference papers, and 3 books/chapters. He was a mid-career Thailand Research Fund scholar from 2013–2015. He currently served as a subcommittee member in the National Research Council of Thailand (NRCT), International Reference Ionosphere (IRI) Committee (under URSI, COSPAR).